PCCP

Cite this: *Phys. Chem. Chem. Phys.*, 2011, **13**, 6947–6954

www.rsc.org/pccp

PAPER

Charge transfer in porphyrin–calixarene complexes: ultrafast kinetics, cyclic voltammetry, and DFT calculations†

Pavel Kubát,*[a] Jakub Šebera,[a] Stanislav Záliš,[a] Jan Langmaier,[a] Marcel Fuciman,[b] Tomáš Polívka[b] and Kamil Lang*[c]

Received 6th September 2010, Accepted 27th January 2011
DOI: 10.1039/c0cp01726d

Transient absorption spectroscopy, cyclic voltammetry, and DFT calculations were used to describe charge transfer processes in a series of 5,10,15,20-tetrakis(*N*-methylpyridinium-*n*-yl) porphyrins (TMPyP*n*, $n = 4,3,2$) and TMPyP*n*/*p*-sulfonatocalix[*m*]arene (clx*m*, $m = 4,6,8$) complexes. Excitation of TMPyP*n* is accompanied by an increasing electron density at the methylpyridinium substituents in the order TMPyP2 < TMPyP3 < TMPyP4. The quenching of the excited singlet states of the complexes increases with the number of ionized phenolic groups of clx*m* and can be correlated with the partial transfer of the electron density from O^- to the peripheral methylpyridinium substituents rather than to the porphyrin ring.

1. Introduction

The photophysical and binding properties of 5,10,15,20-tetrakis(*N*-methylpyridinium-4-yl)porphyrin (TMPyP4, Fig. 1) indicate its use as an efficient photosensitizer in many artificial light-harvesting systems,[1] as well as in medicine for photodynamic therapy (PDT)[2] or the inactivation of bacteria and viruses.[3] Organizing TMPyP4 molecules through noncovalent host–guest interactions with a range of guests including nucleic acids/proteins,[4] calixarenes,[5–9] cyclodextrins,[10] carbon nanotubes,[11] PAMAM dendrimers,[12] graphene,[13] cucurbituril,[14] and their incorporation into micelles,[15] methyl viologen-hybrid,[16] Nafion films,[17] semiconductors,[18] layered silicates,[19,20] hydrogels,[21] and other solid materials is immensely important to the creation of ordered structures of a specific functionality. Isoelectronic TMPyP2 and TMPyP3 (Fig. 1) can modulate the properties of the resulting supramolecular complexes due to the rotational barrier imposed on the methylpyridinium substituents.[7,22]

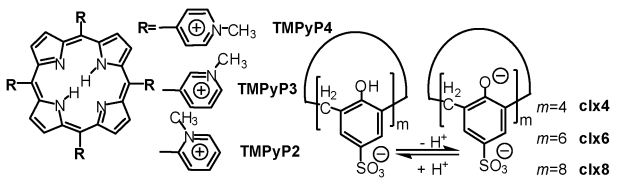

Fig. 1 Structure of porphyrins (TMPyP*n*, $n = 4,3,2$) and *p*-sulfonatocalix[*m*]arenes (clx*m*, $m = 4,6,8$).

Water-soluble *p*-sulfonatocalix[*m*]arenes (Fig. 1) possess three-dimensional, flexible, π electron-rich cavities that can adopt different conformations, form complexes with a variety of compounds,[23] and be used in a diverse array of biomedical applications,[24,25] *e.g.*, as transportation vehicles for porphyrin-based drugs in PDT. The number of conformations increases with the number of 4-hydroxy-benzenesulfonate units in the macrocycle, although this also depends on the solvent and the nature of the guest.

In addition to their biomedical application, TMPyP4-calixarene self-assembled complexes form a highly nanoporous material.[8,9] This supramolecular zeolite-like structure can be easily functionalized by diffusion and coordination of metal ions. Consequently, more detailed information is needed on the photoinduced transfer processes, the quantum yields of the triplet states (Φ_T) and of the singlet oxygen (Φ_Δ) for applications of porphyrin-calixarene systems as light-harvesting materials or in PDT.

In previous papers,[6,7] we have observed strong quenching of porphyrin fluorescence and decrease of Φ_T and Φ_Δ values in Coulombic complexes of TMPyP4 and TMPyP2 with clx*m*. The sub-ns time resolution of fluorescence experiments has not been sufficient to describe the ultrafast dynamics of TMPyP*n* excited states. This paper presents new results concerning the ultrafast transient absorption measurement of TMPyP*n*–clx*m* complexes. The nature of this quenching is discussed on the basis of DFT calculations and electrochemical measurements.

[a] *J. Heyrovský Institute of Physical Chemistry, v.v.i., Academy of Sciences of the Czech Republic, Dolejškova 3, 182 23 Praha 8, Czech Republic. E-mail: kubat@jh-inst.cas.cz; Fax: +420 286582 307; Tel: +420 266053 047*
[b] *Institute of Physical Biology, University of South Bohemia, Zámek 136, 373 33 Nové Hrady, Czech Republic*
[c] *Institute of Inorganic Chemistry, v.v.i., Academy of Sciences of the Czech Republic, 250 68 Řež Czech Republic. E-mail: lang@iic.cas.cz; Fax: +420 220941 502; Tel: +420 266172 193*

† Electronic supplementary information (ESI) available: Acido-basic properties of TMPyP*n* and clx*m*, absorption and transient absorption data, results of DFT calculations. See DOI: 10.1039/c0cp01726d

2. Experimental

Chemicals

5,10,15,20-tetrakis(*N*-methylpyridinium-4-yl) porphyrin tetratosylate (TMPyP4, Aldrich), 5,10,15,20-tetrakis(*N*-methylpyridinium-3-yl)porphyrin tetrachloride (TMPyP3, Frontier Scientific Europe, UK), and 5,10,15,20-tetrakis(*N*-methylpyridinium-2-yl)porphyrin tetratosylate (TMPyP2, Porphyrin Systems, Germany) were used as received. The syntheses of calix[4]arene-*p*-tetrasulfonate (clx4), calix[6]arene-*p*-hexasulfonate (clx6), and calix[8]arene-*p*-octasulfonate (clx8) were described in a previous paper.[6] Experiments were performed in redistilled water and the pH values were adjusted by the addition of NaOH or HCl. The steady-state absorption spectra were measured using a Perkin Elmer Lambda 19 spectrometer.

Femtosecond transient absorption and the analysis of time resolved spectra

The femtosecond transient absorption spectrometer used here has been described in detail elsewhere.[26] Briefly, the second harmonic of the amplifier output (centre wavelength 790 nm) served as a pump beam, resulting in the ~120 fs, 395 nm pulses used for excitation of the samples. Broadband white light pulses generated by focusing a fraction of the amplifier output into a 2 mm sapphire plate were used for probing. All experiments were carried out at the magic angle (54.7°) polarization between excitation and probe beams. For each delay, introduced by a computer-controlled delay line, photo-induced changes in the absorption spectra were detected by dispersing the broadband probe beam onto a 1024-element diode array, resulting in spectro-temporal datasets containing 1024 spectral and 150–250 time points. These datasets were fitted globally using a sequential kinetic scheme.[27]

Voltammetry

The instrumentation consisted of an EG&G PAR potentiostat-galvanostat model 273A equipped with the M270 software. The cell was a three-electrode type with a saturated silver chloride reference electrode (0.222 V *vs.* SHE). A glassy carbon rod served as a counter electrode and a boron-doped diamond disk (surface area 0.0706 cm^2, Windsor Scientific Ltd, UK) was used as a working electrode. Conducting diamond is a chemically inert material and when in contact with liquid electrolyte exhibits very low interfacial capacity. Stock solutions of TMPyP*n* and clx*m* (0.01 M) were prepared by dissolving the appropriate amounts of the compounds in 1 mL of water. They were injected into the cell containing 10 mL of the electrolyte (phosphate buffer, 0.066 M, pH = 7.17) to produce the required concentration (50 μM). Each compound was voltammetrically investigated within the potential window from 1.3 V to −1.3 V with a potential scan rate of 0.05 Vs^{-1}. Experiments were carried out at 25 °C in the absence of oxygen.

3. Computational methods

Ground state DFT calculations of TMPyP*n* (n = 2–4) and TMPyP4–clx*m* (m = 4, 6) were performed using the quantum chemistry packages Gaussian 09[28] and Turbomole 5.10.[29] The 6-31G* polarized double-ζ basis set (G09)[33] and the same quality SVP[34] basis set (Turbomole) for H, C, N, O and S atoms were used. Geometrical optimizations of the ground state and the two lowest singlet excited states of TMPyP*n* were done with B3LYP[30] functional. The hybrid *meta* MPW1B95[31] functional, designed for more accurate description of hydrogen bonding and weak interactions within the DFT method, was used for optimising the geometry of the TMPyP4–clx*m* complexes. Low-lying singlet transitions were calculated by the TD-DFT method on ground state optimized geometries using the identical functional. The conductor-like screening model (COSMO)[32] was used for modelling the influence of the solvent.

DFT calculations were carried out without any symmetry restrictions. The electron density differences were based on the Mulliken population analysis obtained for individual electronic states by TD DFT procedure.

4. Results and discussion

4. 1 TMPyP*n* and clx*m* in solution

Calixarenes clx4, clx6, and clx8 are predominantly penta-, okta-, and deca-anions in neutral aqueous solutions, respectively, due to deprotonation of the sulfonate groups and of one or two of the phenolic OH groups (Table S1 in ESI†).

Ultrafast kinetics. Transient absorption experiments with a time resolution of ~100 fs were carried out by excitation of the porphyrin molecules into their Soret band (S_2 state). Typical transient absorption spectra are shown in Fig. 2 for TMPyP4 in H_2O. The transient absorption spectra consist of ground state bleaching bands at 518, 551, and 583 nm, corresponding to the respective Q absorption bands.[6] A broad, excited-state absorption is superimposed on the bleaching bands and covers the whole measured spectral region. In agreement with other porphyrin-type molecules,[35,36] the intensity of the excited-state absorption increases toward shorter wavelengths. Similar transient absorption spectra were measured for TMPyP3 and TMPyP2 (Fig. S3 in ESI†).

The overall shape of the transient absorption spectrum is conserved during the time window of the experiment (Fig. 2). The similarity of the transient absorption spectra recorded at

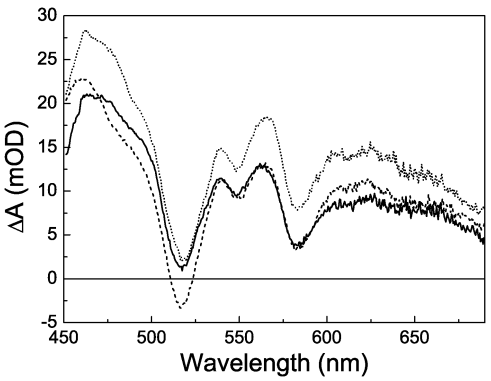

Fig. 2 Transient absorption spectra of TMPyP4 in H_2O (pH 7) measured at different delay times: 0.1 ps (solid line), 0.7 ps (dashed line), and 650 ps (dotted line).

0.1 and 0.7 ps after excitation, and the fact that the spectrum measured at 0.1 ps exhibits the characteristic features of the S_1 state,[36] suggest that the S_2–S_1 relaxation occurs on a sub-150 fs time scale. The maximal difference between the 0.1 and 0.7 ps spectra is observed around 500 nm, and kinetics recorded at this wavelength (data not shown) confirm that the time constant of the S_2–S_1 relaxation is at the limit of our temporal resolution, in agreement with earlier studies that determined the S_2 lifetime to be less than 120 fs.[36,37] Interestingly, although no further changes in the overall shape of the transient absorption spectra are detected, the intensity of the excited-state absorption increases with time, as evidenced by the transient absorption measured at 650 ps (Fig. 2).

Initial ultrafast decay due to the S_2–S_1 relaxation is visible for all TMPyP*n* at 470 nm (Fig. 3). Further dynamics are clearly dependent on the solvent and the structure of the molecule. Except for TMPyP2, which contains only decay components at 470 nm, kinetics exhibit a clear rising component. The rising component is largest for TMPyP4 in H_2O at pH 7 (Fig. 3c). The time constants (τ) of the rising components of the individual samples were determined by global fits of the whole spectro-temporal datasets[27] and are summarized in Table 1. The rising component becomes faster when going from TMPyP3 to TMPyP4 in H_2O at pH 7, and the resulting time constants are 25 and 15 ps, respectively. We also explored the effect of pH on the relaxation dynamics of TMPyP4. The corresponding time constant increases with pH, yielding values of 12, 15, and 22 ps at pH 2, pH 7, and pH 10, respectively (Table 1). Interestingly, the fastest time constant was detected for TMPyP4 in methanol (5 ps). Following this relaxation in the S_1 state, all TMPyP*n* decay with a time constant of 5–14 ns, obtained from fluorescence measurements (Table 1), which is beyond the time window of the transient absorption experiment.

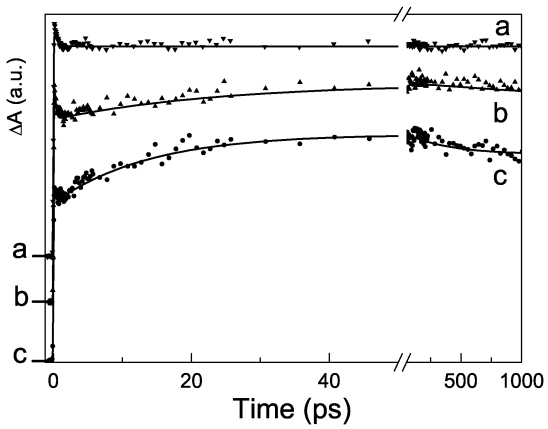

Fig. 3 Kinetics of (a) TMPyP2, (b) TMPyP3, and (c) TMPyP4 in H_2O (pH 7) measured at 470 nm. All kinetics are normalized to the maximum and an offset has been introduced to distinguish individual kinetics.

It should be noted that the results at pH 2 can be influenced by the protonation of TMPyP4 (Table 1). Partial protonation is evidenced by the UV/Vis spectra, which exhibit a shoulder at longer wavelengths (Fig. S2 in ESI†).

DFT calculations. DFT calculations that were recently applied to the estimation of electronic properties of free-base porphyrins and their complexes[39] were used in order to understand the differences in ultrafast kinetics within TMPyP*n*. The calculated spectral parameters, including shifts in the excitation energies caused by the peripheral substitution of the porphyrin ring (Table S3 in ESI†), reproduce well the experimental absorption spectra (Table S2 in ESI†). The Q bands correspond to the transitions from the ground state to the S_1' and S_1'' energy levels, and the Soret band to the almost degenerate S_2' and S_2'' levels.

The rising component observed in the ultrafast measurements (Table 1) can be associated with relaxation of the S_1 states.

Table 1 Decay parameters of TMPyP*n*–clx*m* complexes[a]

System	Solvent	τ_1 [ps] (*A*, %)	τ_2 [ps] (*A*, %)	τ_3 > 1ns (*A*, %)	τ_{fl}[b] [ns]
TMPyP4	H_2O, pH 2	—	12 (*−25*)	(*100*)	—
TMPyP4	H_2O, pH 7	—	15 (*−30*)	(*100*)	6.0[c] 5.1[d]
TMPyP4	H_2O, pH 10	—	22 (*−23*)	(*100*)	—
TMPyP4	MeOH	—	5 (*−12*)	(*100*)	—
TMPyP3	H_2O, pH 7	0.2 (*8*)	25 (*−20*)	(*92*)	7.0[c]
TMPyP2	H_2O, pH 7	0.5 (*5*)	—	(95)	13.8[c] 14.5[d]
TMPyP4-clx4	H_2O, pH 7	0.5(*10*)	20(*−20*)	(*90*)	—
TMPyP4-clx6	H_2O, pH 7	2.0(*50*)	23(*20*)	(*30*)	—
TMPyP4-clx8	H_2O, pH 7	2.0(*40*)	15(*40*)	(*20*)	—
TMPyP4-clx8	H_2O, pH 2	0.7(*10*)	23(*10*)	(*80*)	—
TMPyP4-clx8	H_2O, pH 10	2.0(*50*)	15(*30*)	(*20*)	—
TMPyP3-clx8	H_2O, pH 7	2.7(*30*)	30(*55*)	(*15*)	—
TMPyP2-clx8	H_2O, pH 2	1.5(*30*)	7.0(*20*)	(*50*)	—
TMPyP2-clx8	H_2O, pH 7	2.0(*70*)	7.0(*20*)	(*10*)	—

[a] The time constants are obtained by global fitting all of the spectro-temporal datasets. The amplitudes (*A*) of the individual component shown in parentheses reflect a contribution of each time component in the kinetics at 470 nm. Negative amplitudes correspond to a rise component and denote a fraction of the total rise amplitude (100%), which occurs with the particular time component. The rest of the rise is instantaneous. A fast component with a time constant <120 fs corresponding to depopulation of the Soret band is present in all cases. The longest (τ_3 > 1 ns) component cannot be determined precisely during the temporal window of the experiment. [b] Lifetime from fluorescence experiments. [c] Ref. 38. [d] Ref. 7.

Since the spectral changes associated with this component uniformly increase the excited-state absorption signal in the whole spectral region, it cannot be due to vibrational relaxation, which is usually evidenced by a blue-shift and narrowing of specific hot bands.[40] A rising component was observed in previous studies on TMPyP4,[36] and was hypothesized to be due to conformational relaxation in the S_1 state.

Our DFT calculations reveal changes in the electron density distribution after excitation of TMPyP*n* into the S_1 and S_2 states. Part of the electron density is transferred from the central porphyrin ring to the methylpyridinium peripheral substituents (Table 2), in agreement with a previous qualitative model.[41] The decrease of positive charge on the substituents is larger after excitation into S_2 than into S_1 states. However, in both cases the electron density redistribution decreases in the series TMPy4 > TMPyP3 > TMPyP2. These changes can lead to an increase of the molar absorption coefficients of S_1 absorption on the ps time scale (Fig. 3b,c) that is maximal for TMPyP4, which has the largest electron density redistribution. Furthermore, the fluorescence lifetimes of TMPyP*n* (Table 1) decrease with increasing electron density redistribution.

4.2. TMPyP*n* - clx*m* complexes

Binding of TMPyP*n* to clx*m* leads to a red-shift of the Soret band (Fig. S1 in ESI†), a decrease in the quantum yields of the triplet states, and to a shortening of the fluorescence lifetimes.[6,7] These changes were associated with photoinduced electron transfer within TMPyP*n*–clx*m* complexes and with extended porphyrin aggregation. The complexes were prepared by mixing of TMPyP*n* and clx*m* solutions; the concentration of clx*m* was more than two orders of magnitude higher than that of TMPyP*n*.

Table 2 Changes of the electron density ($\Delta\rho$) on the porphyrin ring in the course of vertical excitation from the ground state (GS) calculated by B3LYP/6-31G*/COSMO for the TMPyP*n* systems. The values calculated in the excited state geometries are in parentheses

System	$\Delta\rho$ (S_1'-GS)	$\Delta\rho$ (S_1''-GS)	$\Delta\rho$ (S_2'-GS)	$\Delta\rho$ (S_2''-GS)
TMPyP2	−0.011 (−0.016)	−0.013 (−0.049)	−0.043	−0.055
TMPyP3	−0.050 (−0.046)	−0.071 (−0.079)	−0.279	−0.327
TMPyP4	−0.088 (−0.111)	−0.135 (−0.175)	−0.366	−0.357

Energetics of photoinduced electron transfer. We recorded redox potentials of TMPyP*n* and clx*m* with the intention of estimating the feasibility of the electron transfer processes (Table 3). The free energy associated with photoinduced electron transfer (ΔG_{et}) can be estimated according to the Rehm–Weller formalism:[42]

$$\Delta G_{et} = E^0_{ox} - E^0_{red} - E^S_{00} - C, \quad (1)$$

where E^0_{ox} and E^0_{red} correspond to the oxidation and reduction potentials of the donor (clx*m*) and acceptor (TMPyP*n*), respectively, and E^S_{00} is the energy of the TMPyP*n* excited singlet state. The term C refers to the Coulombic stabilization energy and can be neglected in the first approximation.

Electrochemical oxidation of clx*m* in aqueous media is complicated by an irreversible process following the oxidation of the phenolate.[43] Products of the reaction passivate the electrode surface[44] and can affect apparent redox potentials $E^{0\prime}(PhO^{\bullet}/PhO^{-})$ derived from the irreversible peak potential (Fig. 4).

Reduction of TMPyP*n* is believed to proceed *via* two-electron transfer steps.[45] The first step is supposed to take

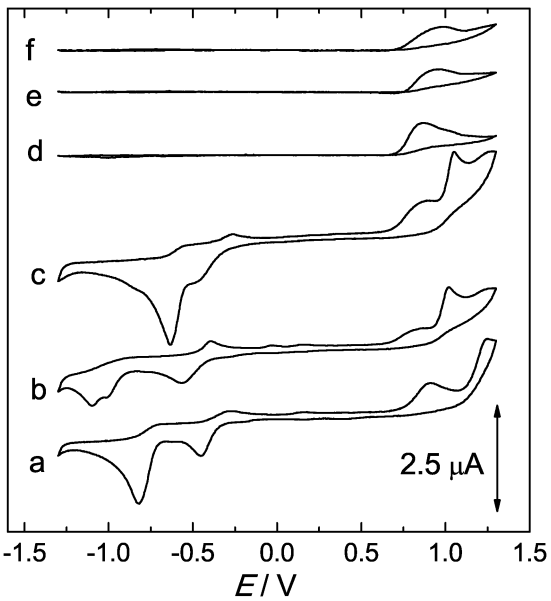

Fig. 4 Cyclic voltammetry responses of (a) TMPyP2, (b) TMPyP3, (c) TMPyP4, (d) clx4, (e) clx6, and (f) clx8 on a diamond electrode; the background has been corrected.

Table 3 Energies of the excited singlet states (E^S_{00}), apparent redox potentials of TMPyP*n* and clx*m* *vs.* Ag/AgCl/saturated KCl estimated by cyclic voltammetry, and the corresponding free energy associated with photoinduced electron transfer (ΔG_{et})

TMPyP*n*	E^S_{00} [eV][a]	$E^{0\prime}$(TMPyP*n*/TMPyP*n*$^{\bullet-}$) [V]	clx*m*	$E^{0\prime}(PhO^{\bullet}/PhO^{-})$ [V]	ΔG_{et} [eV][b]
TMPyP4	1.79	−0.37	clx4	+0.84	−0.58
TMPyP3	1.82	−0.46	clx4	+0.84	−0.52
TMPyP2	1.83	−0.37	clx4	+0.84	−0.62
TMPyP4	1.79	−0.37	clx6	+0.92	−0.50
TMPyP3	1.82	−0.46	clx6	+0.92	−0.44
TMPyP2	1.83	−0.37	clx6	+0.92	−0.54
TMPyP4	1.79	−0.37	clx8	+0.94	−0.48
TMPyP3	1.82	−0.46	clx8	+0.94	−0.42
TMPyP2	1.83	−0.37	clx8	+0.94	−0.52

[a] Lower limit calculated from fluorescence spectra (Table S2 in ESI†). [b] Calculated using eqn (1).

place at the π-ring system to form an unstable π-anion radical, which is disproportionated to phlorin or chlorin. The apparent $E^{0\prime}$(TMPyP*n*/TMPyP*n*$^{\bullet-}$) were estimated as the midpoint potentials of the first TMPyP*n* reduction step, which exhibited quasi-reversible features (Fig. 4).

The values of $E^{0\prime}$(PhO$^{\bullet}$/PhO^{-}), $E^{0\prime}$(TMPyP*n*/TMPyP*n*$^{\bullet-}$), E^{S}_{00}, and calculated ΔG_{et} for photoelectron transfer in the excited singlet states are shown in Table 3. Negative ΔG_{et} values of all TMPyP*n*-clx*m* systems indicate the feasibility of electron transfer between calixarene and porphyrin moieties. It should be noted, however, that these values for ΔG_{et} represent an experimental limit. Faster electron transfer kinetics and/or faster following chemical reactions may only decrease the difference between $E^{0\prime}$(PhO$^{\bullet}$/PhO^{-}) and $E^{0\prime}$(TMPyP*n*/TMPyP*n*$^{\bullet-}$).

Ultrafast kinetics. Comparison of the transient absorption spectra of TMPyP*n* with those of TMPyP*n*–clx*m* complexes does not reveal any additional absorption changes in the recorded range of 450–700 nm (Fig. 2 and Fig. S3, S5 in ESI†) attributable to photoinduced charge transfer in the S_1 state of TMPyP*n*–clx*m* complexes.

Influence of calixarene structure and phenolate anions. In order to explore the effect of ionization of the phenolic OH groups in clx*m* on the transient absorption kinetics, we performed experiments with different calixarenes and/or at different pH levels. Fig. 5 shows kinetics for three TMPyP4–clx*m* complexes in H_2O at pH 7 compared with the relaxation kinetics of TMPyP4. While the TMPyP4–clx4 complex does not exhibit any significant differences (one phenolate anion at pH 7), the increasing number of 4-hydroxybenzenesulfonate units in clx6 (two deprotonated OH groups) clearly induces quenching of the complex S_1 states. This quenching is even more efficient in the TMPyP4–clx8 complex (two deprotonated OH groups) (Table 1).

Detailed analysis shows that both the TMPyP4–clx6 and TMPyP4–clx8 complexes exhibit multi-exponential decay of excited S_1 states. A global fitting analysis reveals that at least four decay components are necessary to get reasonable fits. Time constants extracted from global fitting, together with amplitudes corresponding to the decays measured at 470 nm, are summarized in Table 1. The fastest time component (not listed in Table 1) is at the limits of our temporal resolution and, similarly to the behaviour of pure porphyrins, can be attributed to S_2–S_1 relaxation. Further decay components are 2.0 and 23 ps in TMPyP4–clx6 and 2.0 and 15 ps in TMPyP4–clx8. The slowest decay component is longer than 1 ns and thus impossible to determine in our experiment. The main difference between the complexes with clx6 and those with clx8 lies in the amplitudes of the various components. While the amplitudes of the 2.0 ps component are comparable in both complexes, the amplitude of the 15 ps component in TMPyP4–clx8 increases considerably at the expense of the slow, nanosecond component (Table 1).

We also studied the effect of pH (*i.e.*, the number of O^- groups) on quenching of the S_1 states of the TMPyP4–clx8 complex. The corresponding kinetic curves, measured at pH 2, 7, and 10, are depicted in Fig. 6. It is obvious that quenching of the S_1 states becomes more efficient with the increase of the pH. At pH 2, clx8 is predominantly oktanion with a minor content of one phenolate anion (pK_{a1} = 3.0). However, these results can be affected by partial protonation of the TMPyP4 pyrrole nitrogen atoms (Table 1, Fig. S2 in ESI†). The initial amplitude of the transient absorption signal decreased to only about 60% at 1 ns, demonstrating that this quenching process is significantly slower at this pH than at pH 7. Extracted time constants, listed in Table 1, show that, even at pH 2, there are three decay components, 0.7 ps, 23 ps, and >1 ns, but the longest component dominates, accounting for 80% of the decay.

On the contrary, both of the decay curves at pH 7 and pH 10, characterized by time constants of 2.0 ps, 15 ps, and >1 ns, are dominated by the two faster components (Table 1). The fast overall decay at pH 10 is largely governed by the 2.0 ps component while the 15 ps component is the predominant one at pH 7. It should be noted that clx8 has three to four phenolate anions at pH 10 (pK_{a3} = 8.3 and pK_{a4} = 10.0), but only two anions at pH 7 (pK_{a2} = 4.4).

A similar effect is observed for the TMPyP2–clx8 complex. Quenching is less efficient at pH 2, even though decays at pH 2 and 7 are characterized by the same set of time constants (Table 1 and Fig. S4 in ESI†). At pH 2, the longest (>1 ns) component dominates, while the 2.0 and 7.0 ps components

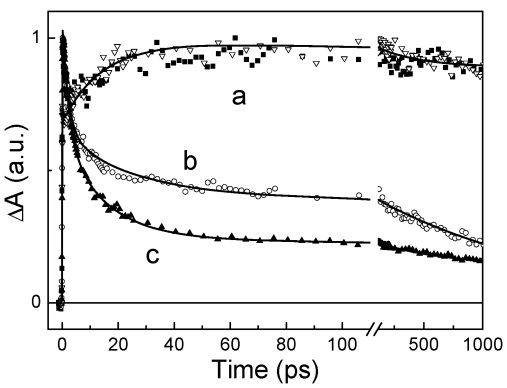

Fig. 5 Kinetics of TMPyP4–clx*m* complexes containing (a) clx4, (b) clx6 and (c) clx8 in H_2O (pH 7) recorded at 470 nm. Kinetics of pure TMPyP4 in H_2O (pH 7) is shown for comparison (open triangles). All kinetics are normalized to the maximum.

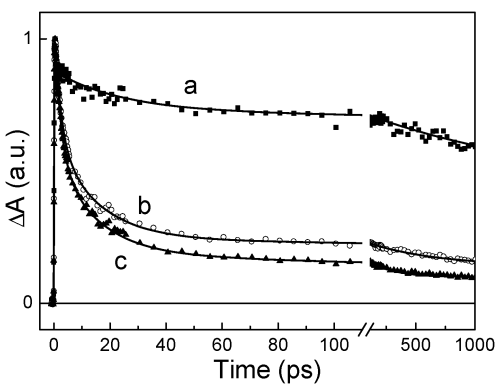

Fig. 6 Kinetics of TMPyP4–clx8 complex measured in H_2O at (a) pH 2, (b) pH 7, and (c) pH 10 as measured at 470 nm. All kinetics are normalized to the maximum.

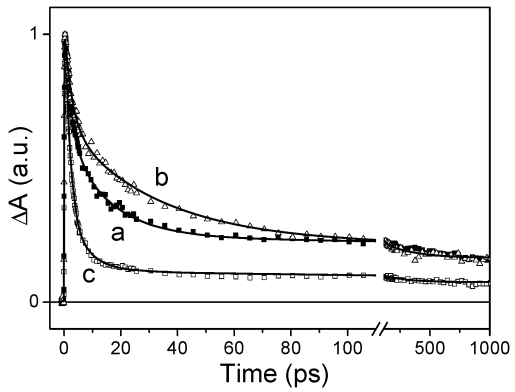

Fig. 7 Kinetics of (a) TMPyP4–clx8, (b) TMPyP3–clx8, and (c) TMPyP2–clx8 complexes measured in H_2O (pH 7) at 470 nm. All kinetics are normalized to the maximum.

account for a majority of the decay at pH 7. At both pH values, however, the overall decay is faster in TMPyP2–clx8 than in TMPyP4–clx8.

Influence of TMPyPn structure. In order to explore the effect of porphyrin isomers, we compared the excited state properties of the TMPyP*n*–clx8 complexes. The multiexponentiality of the decays at 470 nm (Fig. 7) is maintained in all three complexes, but the amplitudes of the individual time components vary significantly. The fastest decay, dominated by a 2.0 ps time constant, which accounts for 70% of the decay, is observed for TMPyP2–clx8. The slower decay observed in TMPyP4–clx8 is due to the predominant component having a time constant of 15 ps (Table 1). Quenching in TMPyP3–clx8 is comparable to that in TMPyP4–clx8, as indicated by the same signal magnitude at 1 ns, but a dominating 30 ps component is obviously slower in TMPyP3–clx8 (Table 1).

The differences in the excited-state dynamics of the complexes of TMPyP*n* positional isomers with clx*m* can be related to the steric and electron-accepting effects of *N*-methylpyridinium substituents including both inductive and mesomeric contributions. The high internal rotation barrier of methylpyridinium substituents in TMPyP2 can contribute to faster decay kinetics (Fig. 7c).

DFT calculations. TD-DFT (MPW1B95/6-31G*/COSMO) calculations were performed using the optimized structures of TMPyP4–clx4 and TMPyP4–clx6 complexes depicted in Fig. 8. Multiexponentiality of the ultrafast kinetics (Table 1) might also indicate the contribution of other geometries. These structures can include different calixarene conformers,

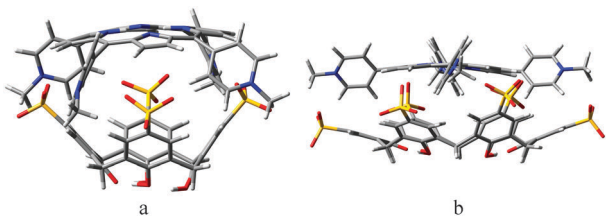

Fig. 8 TD-DFT (MPW1B95/6-31G*/COSMO) optimized geometries of (a) TMPyP4–clx4 and (b) TMPyP4–clx6; both complexes have one ionized O^- group.

Table 4 Changes in the electron density on the porphyrin ring and on the 4-*N*-methylpyridinium (MP) substituents of the TMPyP4 induced by the formation of TMPyP4–clx*m* complexes with a different number of ionized O^- groups, as calculated by MPW1B95/6-31G*/COSMO. $\Delta\rho$(GS), $\Delta\rho(S_1')$, and $\Delta\rho(S_1'')$ are the electron density differences between TMPyP4 in the complex and free TMPyP4 for the ground state (GS) and excited states S_1' and S''_1, respectively

clx*m*	$\Delta\rho$ (GS)		$\Delta\rho$ (S_1')		$\Delta\rho$ (S_1'')	
	Ring	MP	Ring	MP	Ring	MP
	0.000	0.000	−0.063	0.063	−0.092	0.092
clx4	0.062	0.322	−0.023	0.409	−0.047	0.433
clx4_O^- Na^+	0.081	0.329	−0.004	0.416	−0.030	0.443
clx6	0.171	0.381	0.103	0.450	0.084	0.469
clx6_O^- Na^+	0.186	0.415	0.127	0.474	0.104	0.498
clx6_$(O^-)_2$ $(Na^+)_2$	0.181	0.470	0.125	0.529	0.106	0.549

especially those with a larger number of 4-hydroxy-benzenesulfonate units (*i.e.*, clx6, clx8), formation of inclusion complexes, described for the TMPyP4–clx4 system forming star-shaped supramolecular complexes,[8] or different modes of interaction. The description of these structures is beyond the scope of the study. Comparison of calculated S_2' and S_2'' excitation energies for free TMPyP4 and TMPyP4–clx6 (Table S4 in ESI†) shows that TD-DFT reproduces the shift of the Soret band to longer wavelengths due to the complex formation.

The effect of deprotonation of the OH groups was simulated using a TMPyP4–clx6 complex with zero, one, and two phenolate anions. The calculated shift of the Soret band with two deprotonated OH groups (Table S4 in ESI†) does not correspond to an experimentally measured red-shift (Fig. S1 in ESI†). The inclusion of Na^+ counterions corrects this deficiency; therefore, all calculations of deprotonated forms were performed with this counterion.

Table 4 documents that after the formation of complexes, the electron density is partially transferred from the calixarene moiety to the TMPyP4 (mostly to the methylpyridinium substituents) in both the ground and excited states. The changes in electron density $\Delta\rho$ are larger in TMPyP4–clx6 than in TMPyP4–clx4, and the extent of redistribution grows (a) with the number of ionized O^- groups and (b) after excitation to the S_1 states. Because of the complexity of the systems studied, only a qualitative conclusion can be proposed. The quenching kinetics of the S_1 states is evidently related to the extent of electron density transfer within the complex. The larger values of $\Delta\rho$ in Table 4 indicate faster relaxation of the S_1 states. There is no indication of charge transfer states in TMPyP4–clx*m* complexes.

5. Conclusions

In this work, we suggest that ultrafast excited-state dynamics of TMPyP*n* and TMPyP*n*–clx*m* complexes is related to the redistribution of the electron density within these molecular systems. This electronic density redistribution decreases in the series TMPy4 > TMPyP3 > TMPyP2 and the same order is observed for the increase in the molar absorption coefficients of S_1 absorption on the ps time scale. In the case of complexes, partial intramolecular charge separation proceeds predominantly

from the ionized O^- groups of clx*m* to the methylpyridinium peripheral substituents of TMPyP*n*. The redistribution of electron density within TMPyP4–clx*m* (m = 4, 6) complexes in the ground and excited S_1 states increases with the number of ionized O^- groups in clx*m* and can be linked to the increase of quenching efficiency of the S_1 states. The quenching of the S_1 states of TMPyP*n*–clx*m* (n = 2 and 3) might be manifested similarly as in TMPyP4, *i.e.*, electron density transfer to the methylpyridinium substituents. The feasibility of electron transfer is supported by cyclic voltammetry data of individual TMPyP*n* and clx*m*.

Acknowledgements

The authors would like to thank Prof. P. Lhoták (Institute of Chemical Technology, Praha, Czech Republic) for synthesis of the calixarenes. This research was supported by the Czech Science Foundation (P208/10/1678 and 203/09/0691), the Academy of Sciences of the Czech Republic (AV0Z40320502, and AV0Z40400503), and by the Ministry of Education, Youth and Sports (MSM6007665808).

Notes and references

1 P. D. W. Boyd and C. A. Reed, *Acc. Chem. Res.*, 2004, **38**, 235–242.
2 S. Tada-Oikawa, S. Oikawa, J. Hirayama, K. Hirakawa and S. Kawanishi, *Photochem. Photobiol.*, 2009, **85**, 1391–1399; G. Siboni, I. Amit-Patito, E. Weizman, M. Waintraub-Porat, H. Weitman, B. Ehrenberg and Z. Malik, *Cancer Lett.*, 2003, **196**, 57–64.
3 N. A. Romanova, L. Y. Brovko, L. Moore, E. Pometun, A. P. Savitsky, N. N. Ugarova and M. W. Griffiths, *Appl. Environ. Microbiol.*, 2003, **69**, 6393–6398; K. Zupán, M. Egyeki, K. Tóth, A. Fekete, L. Herényi, K. Módos and G. Csík, *J. Photochem. Photobiol., B*, 2008, **90**, 105–112; K. Ergaieg, M. Chevanne, J. Cillard and R. Seux, *Sol. Energy*, 2008, **82**, 1107–1117.
4 R. J. Fiel, *J. Biomol. Struct. Dyn.*, 1989, **6**, 1259–1275; P. Kubát, K. Lang, P. Anzenbacher, K. Jursíková, V. Král and B. Ehrenberg, *J. Chem. Soc., Perkin Trans. 1*, 2000, 933–941; K. Zupán, L. Herényi, K. Tóth, M. Egyeki and G. Csík, *Biochemistry*, 2005, **44**, 15000–15006.
5 G. Moschetto, R. Lauceri, F. G. Gulino, D. Sciotto and R. Purrello, *J. Am. Chem. Soc.*, 2002, **124**, 14536–14537.
6 K. Lang, P. Kubát, P. Lhoták, J. Mosinger and D. M. Wagnerová, *Photochem. Photobiol.*, 2001, **74**, 558–565.
7 P. Kubát, K. Lang, P. Lhoták, P. Janda, J. Sýkora, P. Matějíček, M. Hof, K. Procházka and Z. Zelinger, *J. Photochem. Photobiol., A*, 2008, **198**, 18–25.
8 R. De Zorzi, N. Guidolin, L. Randaccio, R. Purrello and S. Geremia, *J. Am. Chem. Soc.*, 2009, **131**, 2487–2489.
9 F. G. Gulino, R. Lauceri, L. Frish, T. Evan-Salem, Y. Cohen, R. D. Zorzi, S. Geremia, L. D. Costanzo, L. Randaccio, D. Sciotto and R. Purrello, *Chem.–Eur. J.*, 2006, **12**, 2722–2729.
10 J. Mosinger, L. Slavětínská, K. Lang, P. Coufal and P. Kubát, *Org. Biomol. Chem.*, 2009, **7**, 3797–3804.
11 A. S. D. Sandanayaka, R. Chitta, N. K. Subbaiyan, L. D'Souza, O. Ito and F. D'Souza, *J. Phys. Chem. C*, 2009, **113**, 13425–13432; P. Kubát, K. Lang, P. Janda, O. Frank, I. Matulková, J. Sýkora, S. Civiš, M. Hof and L. Kavan, *J. Nanosci. Nanotechnol.*, 2009, **9**, 5795–5802.
12 P. M. R. Paulo and S. M. B. Costa, *J. Phys. Chem. B*, 2005, **109**, 13928–13940; P. Kubát, K. Lang and Z. Zelinger, *J. Mol. Liq.*, 2007, **131–132**, 200–205.
13 Y. Xu, L. Zhao, H. Bai, W. Hong, C. Li and G. Shi, *J. Am. Chem. Soc.*, 2009, **131**, 13490–13497.
14 J. Mohanty, A. C. Bhasikuttan, S. D. Choudhury and H. Pal, *J. Phys. Chem. B*, 2008, **112**, 10782–10785.
15 S. M. Andrade and S. M. B. Costa, *Chem.–Eur. J.*, 2006, **12**, 1046–1057.
16 T. Yui, Y. Kobayashi, Y. Yamada, T. Tsuchino, K. Yano, T. Kajino, Y. Fukushima, T. Torimoto, H. Inoue and K. Takagi, *Phys. Chem. Chem. Phys.*, 2006, **8**, 4585–4590.
17 Y. Itagaki, S. Nakashima and Y. Sadaoka, *Sens. Actuators, B*, 2009, **142**, 44–48.
18 S. Qiu, L. Sun, H. Chu, Y. Zou, F. Xu and N. Matsuda, *Thin Solid Films*, 2009, **517**, 2905–2911.
19 A. Čeklovský, A. Czímerová, K. Lang and J. Bujdák, *J. Lumin.*, 2009, **129**, 912–918.
20 Z. Chernia and D. Gill, *Langmuir*, 1999, **15**, 1625–1633.
21 C. Brady, S. E. J. Bell, C. Parsons, S. P. Gorman, D. S. Jones and C. P. McCoy, *J. Phys. Chem. B*, 2007, **111**, 527–534.
22 F. X. Han, R. T. Wheelhouse and L. H. Hurley, *J. Am. Chem. Soc.*, 1999, **121**, 3561–3570.
23 D.-S. Guo, K. Wang and Y. Liu, *J. Inclusion Phenom. Macrocyclic Chem.*, 2008, **62**, 1–21.
24 W. Yang, D. P. Otto, W. Liebenberg and M. M. de Villiers, *Curr. Drug Discovery Technol.*, 2008, **5**, 129–139.
25 F. Perret, A. N. Lazar and A. W. Coleman, *Chem. Commun.*, 2006, 2425–2438.
26 P. Chábera, M. Fuciman, P. Hříbek and T. Polívka, *Phys. Chem. Chem. Phys.*, 2009, **11**, 8795–8803.
27 I. H. M. Van Stokkum, D. S. Larsen and R. Van Grondelle, *Biochim. Biophys. Acta, Bioenerg.*, 2004, **1657**, 82–104.
28 M. J. Frisch, G. W. Trucks, H. B. Schlegel, G. E. Scuseria, M. A. Robb, J. R. Cheeseman, G. Scalmani, V. Barone, B. Mennucci, G. A. Petersson, H. Nakatsuji, M. Caricato, X. Li, H. P. Hratchian, A. F. Izmaylov, J. Bloino, G. Zheng, J. L. Sonnenberg, M. Hada, M. Ehara, K. Toyota, R. Fukuda, J. Hasegawa, M. Ishida, T. Nakajima, Y. Honda, O. Kitao, H. Nakai, T. Vreven, J. A. Montgomery, Jr., J. E. Peralta, F. Ogliaro, M. Bearpark, J. J. Heyd, E. Brothers, K. N. Kudin, V. N. Staroverov, R. Kobayashi, J. Normand, K. Raghavachari, A. Rendell, J. C. Burant, S. S. Iyengar, J. Tomasi, M. Cossi, N. Rega, J. M. Millam, M. Klene, J. E. Knox, J. B. Cross, V. Bakken, C. Adamo, J. Jaramillo, R. Gomperts, R. E. Stratmann, O. Yazyev, A. J. Austin, R. Cammi, C. Pomelli, J. Ochterski, R. L. Martin, K. Morokuma, V. G. Zakrzewski, G. A. Voth, P. Salvador, J. J. Dannenberg, S. Dapprich, A. D. Daniels, O. Farkas, J. B. Foresman, J. V. Ortiz, J. Cioslowski and D. J. Fox, *GAUSSIAN 09 (Revision A.2)*, Gaussian, Inc., Wallingford, CT, 2009.
29 R. Ahlrichs, M. K. Armbruster, M. Bär, H.-P. Baron, R. Bauernschmitt, S. Böcker, N. Crawford, P. Deglmann, M. Ehrig, K. Eichkorn, S. Elliott, F. Furche, F. Haase, M. Häser, Ch. Hättig, A. Hellweg, H. Horn, Ch. Huber, U. Huniar, M. Kattannek, A. Köhn, Ch. Kölmel, M. Kollwitz, K. May, P. Nava, Ch. Ochsenfeld, H. Öhm, H. Patzelt, D. Rappoport, O. Rubner, A. Schäfer, U. Schneider, M. Sierka, O. Treutler, B. Unterreiner, M. von Arnim, F. Weigend, P. Weis and H. Weiss, TURBOMOLE V5-10, Quantum Chemistry Group, University of Karlsruhe, Karlsruhe, Germany, 2008.
30 P. J. Stephens, F. J. Devlin, C. F. Chabalowski and M. J. Frisch, *J. Phys. Chem.*, 1994, **98**, 11623–11627.
31 Y. Zhao and D. G. Truhlar, *Acc. Chem. Res.*, 2008, **41**, 157–167.
32 A. Klamt, *J. Phys. Chem.*, 1996, **100**, 3349–3353.
33 P. C. Hariharan and J. A. Pople, *Theor. Chim. Acta*, 1973, **28**, 213–222.
34 A. Schafer, H. Horn and R. Ahlrichs, *J. Chem. Phys.*, 1992, **97**, 2571–2577.
35 J. Larsen, B. Bruggemann, T. Polívka, V. Sundstrom, E. Akesson, J. Sly and M. J. Crossley, *J. Phys. Chem. A*, 2005, **109**, 10654–10662.
36 K. Steenkeste, M. Enescu, F. Tfibel, P. Pernot, S. Far, M. Perrée-Fauvet and M. P. Fontaine-Aupart, *Phys. Chem. Chem. Phys.*, 2004, **6**, 3299–3308.
37 K. Y. Yeon, D. Jeong and S. K. Kim, *Chem. Commun.*, 2010, **46**, 5572–5574.
38 K. Kalyanasundaram, *Inorg. Chem.*, 1984, **23**, 2453–2459.
39 X. Ren, A. Ren, J. Feng and C. Sun, *J. Photochem. Photobiol., A*, 2009, **203**, 92–99; M. Nardi, R. Verucchi, C. Corradi, M. Pola,

M. Casarin, A. Vittadini and S. Iannotta, *Phys. Chem. Chem. Phys.*, 2010, **12**, 871–880; M.-S. Liao, J. D. Watts and M.-J. Huang, *Phys. Chem. Chem. Phys.*, 2009, **11**, 4365–4374; F. Santoro, A. Lami, R. Improta, J. Bloino and V. Barone, *J. Chem. Phys.*, 2008, **128**, 224311.
40 H. H. Billsten, D. Zigmantas, V. Sundström and T. Polívka, *Chem. Phys. Lett.*, 2002, **355**, 465–470.
41 F. J. Vergeldt, R. B. M. Koehorst, A. van Hoek and T. J. Schaafsma, *J. Phys. Chem. A*, 1995, **99**, 4397–4405.
42 D. Rehm and A. Weller, *Isr. J. Chem.*, 1970, **8**, 259–267.
43 A. Pailleret, N. Magan-Oliva, S. Ollivier and D. W. M. Arrigan, *J. Electroanal. Chem.*, 2001, **508**, 81–88; G. Diao and W. Zhou, *J. Electroanal. Chem.*, 2004, **567**, 325–330.
44 A. Pailleret, G. Herzog and D. W. M. Arrigan, *Electrochem. Commun.*, 2003, **5**, 68–72.
45 M. C. Richoux, P. Neta, A. Harriman, S. Baral and P. Hambright, *J. Phys. Chem.*, 1986, **90**, 2462–2468; E. Van Caemelbecke, A. Derbin, P. Hambright, R. Garcia, A. Doukkali, A. Saoiabi, K. Ohkubo, S. Fukuzumi and K. M. Kadish, *Inorg. Chem.*, 2005, **44**, 3789–3798.

